A Multigrid Algorithm for Steady Transonic Potential Flows Around Aerofoils Using Newton Iteration*

J. W. BOERSTOEL

National Aerospace Laboratory NLR, Amsterdam, The Netherlands

The application of multigrid relaxation to transonic potential-flow calculation was investigated. Fully conservative potential flows around aerofoils were taken as test problems. The solution algorithm was based on Newton iteration. In each Newton iteration step, multigrid relaxation was used to calculate correction potentials. It was found that the iteration to the circulation has to be kept outside the multigrid algorithm. In order to obtain meaningful norms of residuals (to be used in termination tests of loops), difference formulas with asymptotic scaling were introduced. Nonlinear instability problems were solved by upwind differencing using mass-flux-vector splitting instead of artificial viscosity or artificial density. It was also found that the multigrid method cannot efficiently update shock positions due to the (mainly) linear character of individual multigrid relaxation cycles. For subsonic flows, the algorithm is quite efficient. For transonic flows, the algorithm was found robust; it efficiency should be increased by improving the iteration on the shock positions; this is a highly nonlinear process.

1. INTRODUCTION

Most computer codes for the calculation of transonic potential flows are based on the solution of a large finite-difference equation system by some nonlinear relaxation algorithm. The development of these algorithms started about a decade ago with work of Murman and Cole, who applied upwind differencing in supersonic zones to generate directional bias [1]. The most important improvements since then were the introduction of the concept of full discrete conservation [2], the extension to the full nonlinear potential-flow equation [3], and the application of results of tensor theory to allow nonorthogonal curvilinear grids so that grids can be easily aligned with complex flow boundaries [4, 5]. An impression of the state of the art may be obtained from [6, 7].

During the last few years, numerical analysts have proposed various new fast-solver algorithms that perhaps may also be used to solve finite-difference equations for transonic potential flow more efficiently than nonlinear relaxation algorithms. The

314

most interesting fast solvers are CR/FFT (cyclic reduction/fast Fourier transformation), AF (approximate factorization), ILU (incomplete lower-upper decomposition), and MGR (multigrid relaxation). For transonic potential-flow calculations, fast solvers of wide applicability are of particular interest because of the complexity of the potential-flow equation (nonlinear, of elliptic–hyperbolic type, singular at shocks and sonic lines).

The application of multigrid methods to transonic potential-flow calculations was investigated by several authors [8–13]. Interesting results were obtained by Fuchs for two-dimensional transonic small-perturbation flow around nonlifting symmetrical aerofoils. Some combinations of the various finite-difference equation systems and various versions of multigrid relaxation algorithms tested by Fuchs turned out to be very efficient. The other authors also reported promising results. Approximate factorization techniques have also been applied with success [14–16]. As a function of the number of grid points, approximate factorization is theoretically asymptotically slower than multigrid relaxation, however. As yet, ILU methods have not been applied to transonic problems. The application of CR/FFT to transonic flow problems turned out to be not quite successful.

The present study concerns the design of a fast-solver algorithm for transonic potential-flow calculations using Newton iteration and multigrid relaxation.

From preliminary investigations it was known that Newton iteration (exact or approximate) was promising [8, 9, 17, 18]. The Newton iteration technique was also proposed by Hackbusch to solve other nonlinear problems than transonic problems [19].

Within each Newton iteration step, a linear correction problem has to be solved. This is done with multigrid relaxation. Various multigrid relaxation algorithms exist [20, 21]: for example, a nonlinear version known as the FAS (full approximation storage) method, and a linear version known as the cycle C method. In this study, the linear version was applied because the convergence analysis is considerably simpler.

Two-dimensional full potential flow around an arbitrary given aerofoil was used as a test problem. The flow equations were discretized in a fully conservative manner on an approximately orthogonal gird of O type. The grid is aligned along the aerofoil.

The nonlinear finite-difference equations are presented in Section 2, the main structure of the solution algorithm in Section 3, the multigrid process in Section 4, and the relaxation technique applied in the multigrid process in Section 6. Results of numerical experiments and a concluding discussion form the last two sections. Some stability considerations are presented in Section 5.

2. FINITE-DIFFERENCE EQUATIONS

The finite-difference equations to be solved are defined on a grid of O type. Such a grid may be generated by a mapping from an equidistant grid in a computational ξ-η plane to the physical x-y plane. The mapping used here consists of a sequence of a few simple transformations, illustrated in Fig. 1: a conformal Karman–Trefftz
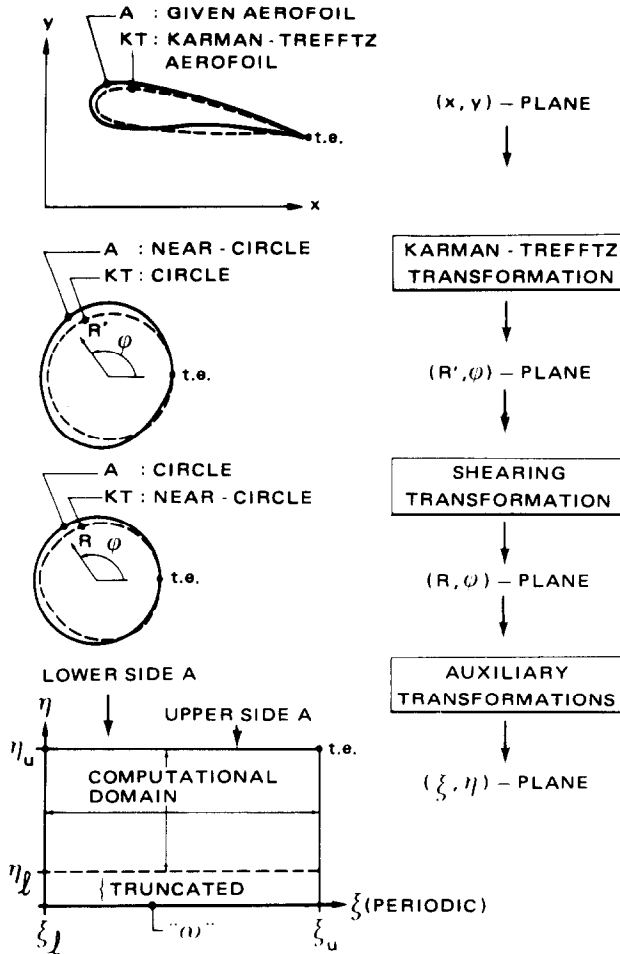
FIGURE 1

transformation followed by simple correction transformation. A Karman–Trefftz aerofoil is (crudely) fitted to the aerofoil such that the aerofoil becomes a smooth near-circle under the corresponding Karman–Trefftz transformation. The trailing-edge corner is thereby removed. The subsequent transformations map the aerofoil into a circle (stretching and shearing in radial direction), and introduce a stretching far from the aerofoil in a direction approximately normal to the streamlines, with a stretch factor $(1 - M_\infty^2)^{1/2}$. Near the trailing edge, the total mapping was designed to be conformal to first order in $(\eta - \eta_u)$; this permits easy implementation of various forms of the Kutta condition. (See also Fig. 2.)

An example of a grid is presented in Fig. 3. As shown, the grid is truncated far from the aerofoil (4–10 chords).
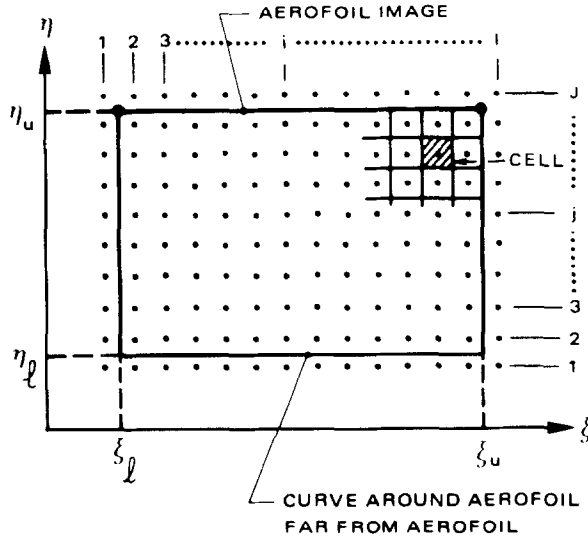
FIGURE 2

Because, in fast-solver algorithms, the corrections to given approximate solutions are in general much greater than the (usually small and smooth) corrections in nonlinear relaxation algorithms, fast-solver algorithms are considerably more prone to nonlinear instability. In the initial stages of the study it was found that various forms of artificial viscosity terms often gave rise to expansion shocks, particularly on coarser grids and also at tops of supersonic zones. A nonlinear finite-difference equation system with excellent stability properties was obtained by introducing directional bias with mass-flux-vector splitting; this is a generalization to full potential flow of a concept applied by Engquist and Osher to stabilize the fully-conservative difference equations for transonic small-perturbation flow [22]. Numerical experiments revealed that it was also necessary to compute the density at cell-face centres instead of at cell corners. (Computation of the density at cell corners is the usual practice in most computer codes.)

The finite-difference equation for the mass conservation equation of each cell (i, j) on the computational plane has the form ($\cdot^{\mathrm{T}}$ means transposition) (see Fig. 4)

$$\nabla_{i,j}^{\mathrm{T}} F^d = 0, \tag{1}$$

where ∇ is a second-order accurate discretization of the gradient operator $(\partial/\partial\xi, \partial/\partial\eta)$; see below for details. We denote by F^d a discrete mass-flux vector with three components (hence, the term mass-flux-vector splitting):

$$F^d = F - F^a + F^{ar}, \tag{2}$$
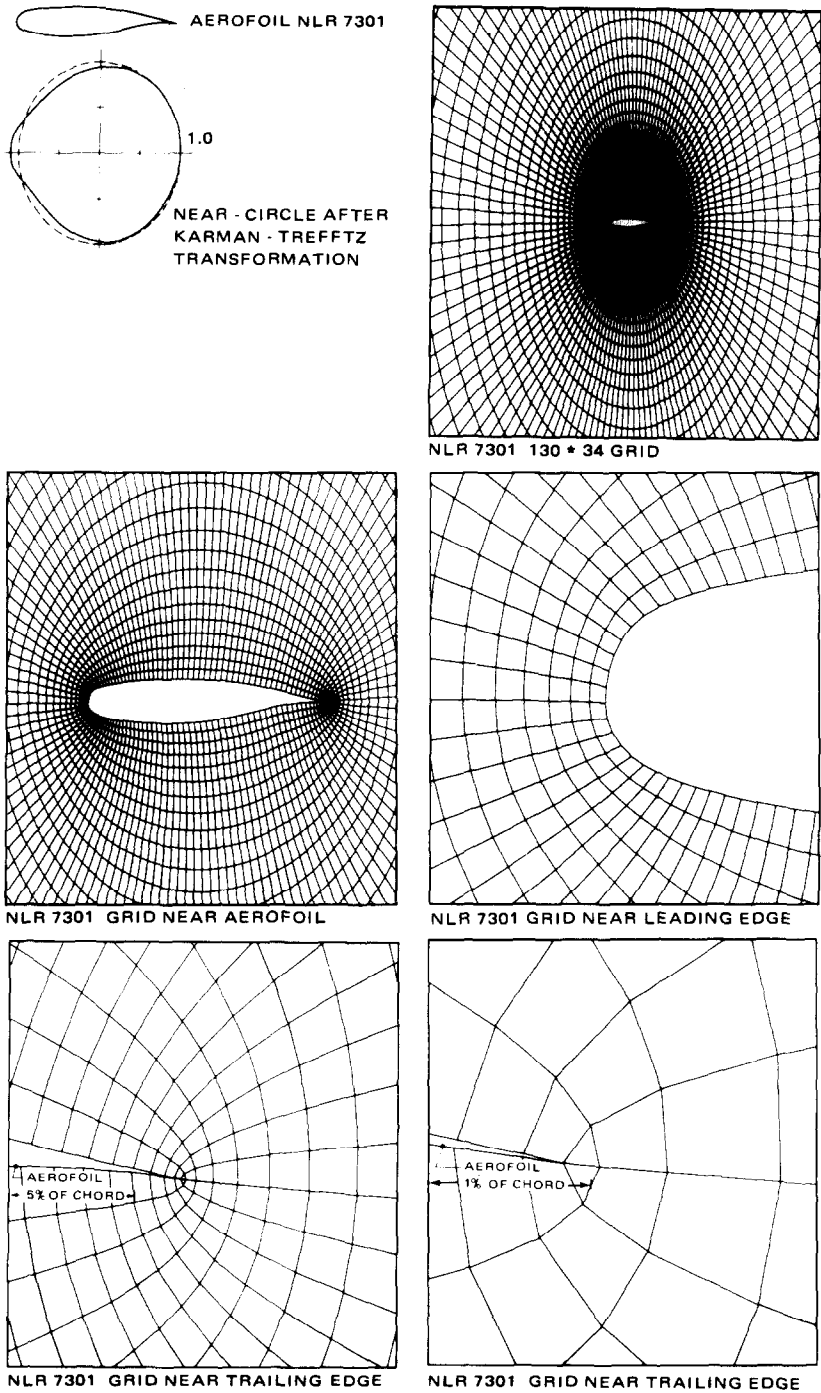
with F the usual mass-flux vector:

AEROFOIL NLR 7301

1.0

NEAR - CIRCLE AFTER
KARMAN - TREFFTZ
TRANSFORMATION

NLR 7301 130 * 34 GRID

NLR 7301 GRID NEAR AEROFOIL

NLR 7301 GRID NEAR LEADING EDGE

AEROFOIL
5% OF CHORD

NLR 7301 GRID NEAR TRAILING EDGE

AEROFOIL
1% OF CHORD

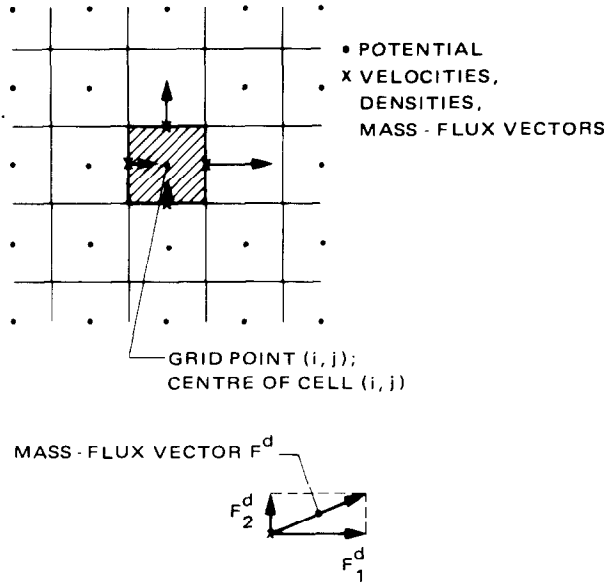NLR 7301 GRID NEAR TRAILING EDGE

FIGURE 3

FIGURE 4

$$F = \rho h U, \tag{3}$$

$$U = G \, \nabla\varphi, \tag{4}$$

$$\rho = \{1 - \tfrac{1}{2}(\gamma - 1)\, M_\infty^2 (1 - q^2)\}^{1/(\gamma-1)}, \tag{5}$$

$$q^2 = (\nabla\varphi)^{\mathrm{T}} G \, \nabla\varphi. \tag{6}$$

Here G is the contravariant metric tensor and h the determinant of the mapping $(\xi, \eta) \rightarrow (x, y)$. Velocities q and desities ρ have been scaled by their free-stream values. The mass-flux vector F^a is nonzero in supersonic zones

$$F^a = 0, \qquad\qquad\qquad \text{if} \quad M \leqslant 1,$$

$$= \{(\rho q - \rho^* q^*)/q\} \, h(UU^{\mathrm{T}}/q^2) \, \nabla\varphi, \qquad \text{otherwise}, \tag{7}$$

where M is the local Mach number, ρ^* and q^* the sonic values of the density and the speed, and UU^{T} is the 2×2 matrix defined by the exterior product of U with itself. The mass-flux vector F^{ar} is equal to F^a at the centre of the upstream cell-face. (F^d will be computed at centres of cell faces).

The components of the mass-flux vectors F and F^a are computed at the centres of cell faces with second-order accurate central-difference and central-averaging formulas applied to φ. The Mach number test involved in the calculation of F^a is also made at the cell-face centres; this implies that the Mach number test for F^{ar} is made at the upstream cell-face centre; it will be seen below that this has interesting conse-

quences for the construction of sonic and shock operators. The metric data are assumed to be known at the cell-face centres.

Physical and mathematical properties of the mass-flux vectors and their discrete divergences are readily obtained by decomposing the matrices G and (UU^{T}/q^2) using the orthonormal matrix

$$V = \begin{bmatrix} \varphi_x/q & -\varphi_y/q \\ \varphi_y/q & \varphi_x/q \end{bmatrix} = \begin{bmatrix} x_s & x_n \\ y_s & y_n \end{bmatrix}, \qquad VV^{\mathrm{T}} = \text{unit matrix}, \qquad (8)$$

and the relation $G = H^{-1}H^{-1\mathrm{T}}$, H the Jacobian of the mapping from the computational space to the physical space. In (8), (s, n) are the natural coordinates of the flow. In particular, F, F^a, and $F - F^a$ depend on mass-flux vectors in natural coordinates as follows if $M \geqslant 1$:

$$F = hH^{-1}V[\rho\varphi_s, \rho\varphi_n]^{\mathrm{T}}, \qquad (9)$$

$$F^a = hH^{-1}V[\rho\varphi_s - \rho^*q^*, 0]^{\mathrm{T}}, \qquad (10)$$

$$F - F^a = hH^{-1}V[\rho^*q^*, \rho\varphi_n]^{\mathrm{T}}. \qquad (11)$$

These expressions show that, in supersonic zones and in natural coordinates, the streamline component of $F - F^a$ has a fixed sonic magnitude; the other component is zero because $\varphi_n = 0$. Because the scalar $\rho q = \rho\varphi_s$, as a function of the speed $q = \varphi_s$, has a maximum at the sonic speed q^*, the vector F^a measures the mass-flux excess in comparison to the sonic maximum mass flux ρ^*q^*. Although $F - F^a$ is a vector of fixed magnitude in natural coordinates, its divergence is generally nonzero (φ_{nn} is not identically zero); this divergence is a measure of the convergence of the streamlines.

It may be shown that, in smooth parts of supersonic zones, the implicit artificial viscosity generated by the divergence of $F^a - F^{ar}$ is closely related to that of Jameson [3], and to the viscosity encountered in the artificial density used by Eberle [25], Hafez et al. [26], and Holst [14]. At sonic lines and at shocks, the relation between the vector-split concept and the artificial-viscosity and artificial-density concepts is lost, however.

At sonic lines, expansion shocks cannot occur because the mass-flux vector F^d is forced to have a sonic magnitude:

$$F^d = hH^{-1}V[\rho^*q^*, \rho\varphi_n]^{\mathrm{T}}, \qquad F^a \neq 0, \qquad F^{ar} = 0, \qquad (12)$$

at the first supersonic cell-face centre after the sonic line. Approximately normal shocks are allowed to become very steep, mainly because, at the first subsonic cell-face centre after the sonic line in the shock, the mass-flux vector F^d has the special value

$$F^d = F + F^{ar}, \qquad F = \rho hU, \qquad F^{ar} \neq 0 \qquad \text{because} \quad M^r > 1. \qquad (13)$$

It may be shown that the finite-difference equations for transonic small-perturbation

flow proposed by Engquist and Osher have simular properties. They showed that their difference formulas have stable and unique solutions [23]. The concept of mass-flux-vector splitting presented here is a formal generalization to the full nonlinear flow equation of their splitting.

The precise definition of the discrete gradient operators ∇ in Eqs. (1), (4), and (7) differs from the usual ones because asymptotic scaling is applied. This has been done to obtain useful norms of residuals to be used in termination tests of iteration loops. Because of the grid stretching and the singular behaviour of the potential near free-stream infinity, the residuals of sufficiently accurate approximate solutions need not be uniformly small over the entire grid, but are allowed to have a certain growth rate when tending to free-stream infinity. Efficient residual norms should account for the permitted growth rate. On O-type grids the permitted growth rate may be analyzed if finite-difference formulas with asymptotic scaling are applied.

Asymptotic scaling naturally emerges on O-type grids if we require that the velocity must be approximated uniformly to $O(h^m)^2$ (h^m mesh size) for any sufficiently smooth potential φ having the expected asymptotic behaviour when tending to infinity ($\eta \downarrow 0$). This requirement leads to an analysis of the relation between approximation errors of difference formulas and the asymptotic behaviour for $\eta \downarrow 0$ of all kinds of functions of (ξ, η), such as potentials, metric data, mass-flux vectors, and residues.

The main steps of the analysis are the following: The mapping from the computational to the physical plane is defined such that

$$x = \eta^{-1} \cos 2\pi\zeta + \cdots,$$
$$\beta y = \eta^{-1} \sin 2\pi\zeta + \cdots, \tag{14}$$

$$\varphi = \eta^{-1}\bar{c}_\infty(\zeta) + \Gamma d_\infty(\zeta) + \cdots, \tag{15}$$

$$\zeta = (\xi - \xi_l)/(\xi_u - \xi_l) + \text{const}, \tag{16}$$

$$\beta = (1 - M_\infty^2)^{1/2}. \tag{17}$$

Using these formulas, it may be shown that the metric constants in expression (6) for q^2,

$$q^2 = (\nabla\varphi)^{\mathrm{T}} G \nabla\varphi = g^{11}\varphi_\xi^2 + 2g^{12}\varphi_\xi\varphi_\eta + g^{22}\varphi_\eta^2 \tag{18}$$

and the derivatives of the potential have asymptotic magnitudes given by

$$g^{11} = O(\eta^2), \qquad g^{12} = O(\eta^3), \qquad g^{22} = O(\eta^4),$$
$$\varphi_\xi = O(\eta^{-1}), \qquad \varphi_\eta = O(\eta^{-2}). \tag{19}$$

It follows that q may be approximated with an absolute accuracy of $O(h^m)^2$, indeed, if φ_ξ and φ_η are approximated by difference formulas with an absolute accuracy of the order $\eta^{-1}(h^m)^2$ and $\eta^{-2}(h^m)^2$, respectively.

In general, difference formulas for derivatives f_η of functions $f(\xi, \eta)$ having an asymptotic power series of the form

$$f(\xi, \eta) = c_0(\xi)\, \eta^{-q} + c_1(\xi)\, \eta^{-q+1} + \cdots \tag{20}$$
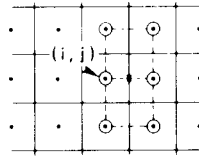
may be derived from the identity

$$f_\eta = \{(\eta^{q+1}f)_\eta - (q+1)\, \eta^q f\}\, \eta^{-q-1} \tag{21}$$

by applying the usual central-difference formulas to the terms $(\eta^{q+1}f)$ and $(\eta^q f)$, because these terms are of unit order in η. The resulting difference formulas are a mixture of numerical and analytical differentiation in η, and have an absolute accuracy of order $\eta^{-q-1}(h^m)^2$.
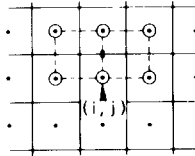
These general considerations were used to define the discrete gradient operators ∇ as follows: Indicate the usual averaging and first-order difference operators by μ_ξ, μ_η, δ_ξ, δ_η, with

$$\mu_{\xi(i,j)}f = \tfrac{1}{2}(f_{i+1/2,j} + f_{i-1/2,j}), \qquad \delta_{\xi(i,j)}f = (f_{i+1/2,j} - f_{i-1/2,j})/h^m, \tag{22}$$
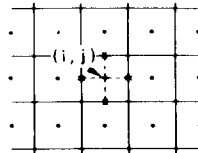
then (see Fig. 5 for the stencils)

STENCIL OF $\nabla_{i+1/2,j}\, ()$

STENCIL OF $\nabla_{i,j+1/2}\, ()$

STENCIL OF $\nabla^T_{i,j}\, F_d$

FIGURE 5

$$\nabla_{i,j}^{T} F^{d} = [\delta_{\xi} F_{1}^{d} + \{\delta_{\eta}(\eta^{2} F_{2}^{d} - 2\eta\mu_{\eta}(\eta F_{2}^{d})\} \, \eta^{-2}]_{i,j}, \tag{23}$$

$$\nabla_{i+1/2,j}\varphi = [\delta_{\xi}\varphi, \, \{\mu_{\eta} \, \delta_{\eta}(\eta^{2}\eta_{\xi}\varphi) - 2\eta\mu_{\xi}\varphi\} \, \eta^{-2}]_{i+1/2,j}^{T}, \tag{24}$$

$$\nabla_{i,j+1/2}\varphi = [\mu_{\xi} \, \delta_{\xi}\{\eta^{-1}\mu_{\eta}(\eta\varphi)\}, \, \{\delta_{\eta}(\eta^{2}\varphi) - 2\eta\mu_{\eta}(\eta\varphi)\} \, \eta^{-2}]_{i,j+1/2}^{T}. \tag{25}$$

Asymptotic scaling is also applied in the retarded mass-flux vectors F^{ar}, when retardation in the η direction has to occur

$$F_{i,j+1/2}^{ar} = [F_{1(i,j+1/2-\alpha)}^{a}(\eta_{j+1/2}^{2}/\eta_{j+1/2-\alpha}^{2}), F_{2(i,j+1/2-\alpha)}^{a}(\eta_{j+1/2}/\eta_{j+1/2-\alpha})]^{T}. \tag{26}$$

The Neumann boundary condition on the aerofoil surface is zero mass flux through the aerofoil surface. This condition has been implemented in two linearly independent ways in the finite-difference equation system:

(i) The mass-conservation equation (1), (23) of each cell $(i, J - 1)$ adjacent to the aerofoil image is modified by requiring that no mass enters the cell through the cell face $(i, J - \frac{1}{2})$ on the aerofoil image:

$$F_{2(i,J-1/2)}^{d} = 0. \tag{27}$$

(ii) The potential values $\varphi_{i,J}$ inside the aerofoil are coupled to the potential values in the flow field by applying the boundary condition at each cell-face centre $(i, J - \frac{1}{2})$ on the aerofoil in the form

$$F_{2(i,J-1/2)} = 0; \tag{28}$$

F^{a} and F^{ar} are thus not used in this boundary condition, so that a second row of potential values inside the aerofoil is not needed.

The Dirichlet boundary condition is applied on a large closed curve $\eta = \eta_{l}$ around the aerofoil (in calculations, 4–10 chords from the aerofoil):

$$\varphi_{i,3/2} = \bar{x}_{i,3/2} - (\Gamma/2\pi) \arctan(\beta\bar{y}/\bar{x})_{i,3/2}, \tag{29}$$

$$\bar{x} = x \cos \alpha_{\infty} + y \sin \alpha_{\infty}, \tag{30}$$
$$\bar{y} = -x \sin \alpha_{\infty} + y \cos \alpha_{\infty},$$

with α_{∞} the free-stream incidence. Because the potential values are given on the free-stream boundary $j = \frac{3}{2}$ instead of at the grid points $(i, 1)$, one-sided second-order accurate difference formulas have been used at the free-stream boundary instead of the central formulas (24, 25).

The circulation Γ is determined by the Kutta condition. Because near the trailing edge the grid is approximately conformal, the Kutta condition may be given the form $(\varphi_{\xi})_{\text{te}} = 0$ if the flow is subsonic at the trailing edge. We approximate $(\varphi_{\xi})_{\text{te}}$ by a central-difference formula.

3. SOLUTION ALGORITHM

The nonlinear finite-difference equation system is solved by a fast-solver algorithm based on the combined use of Newton iteration and multigrid relaxation. The main structure of this algorithm is presented in this section.

During the study it was found that due attention has to be paid to a few new problems:

(i) Circulation changes in general give rise to an increase of norms of residuals. In order to prevent limit cycling or divergence of nested iteration processes (here, Newton iteration and multigrid relaxation), the increase must be allowed for in termination criteria of iteration loops.

(ii) The solution algorithm has to iterate on different types of nonlinearity: a short-wavelength nonlinearity at shocks with a length scale of the order of one mesh of the finest grid in a current grid sequence, and a mild nonlinearity elsewhere with length scales of geometric properties of the aerofoil such as the chord or the leading-edge radius. The short-wavelength nonlinearity is encountered during shock-position improvements. Both types of nonlinearity have to be processed after each circulation improvement because circulation changes give rise to changes far from the aerofoil (almost linear, length-scale the chord), at the leading edge (mildly nonlinear, length scale l.e. radius), and at shocks (strongly nonlinear, length scale the mesh of the finest grid).

It was also found that multigrid processes do not efficiently improve shock positions on fine grids if the shocks have to move over several (say five) meshes of such grids. (Such movements easily may be required by circulation updates, for example.) This may be explained as follows: Multigrid relaxation is based on the assumption that a correction to an approximate solution may be decomposed into a sum of short-wavelength and long-wavelength components; the short-wavelength components are (efficiently) computed on the finest grid of a grid sequence, and the long-wavelength components are computed on coarser grids where fewer grid points are involved in the calculations. Such a linear decomposition of a correction grid function in short- and long-wavelength components has sense in linear problems and also in linearizations of nonlinear problems. Linearizations of the shock operators, however, can at best estimate shock movements over one mesh of the finest grid. In fast-solver algorithms the shock should be able to move over several meshes, however. The basic assumption of linearity of the multigrid relaxation process thus conflicts with the nonlinearity of the shock-movement process. (This is also true for the nonlinar FAS–multigrid relaxation method proposed by Brandt [21], because Brandt's construction of the FAS method makes use of the linearity of the correction problem on the finest grid.) Other details concerning multigrid relaxation and shock position updates are presented in Fig. 6.

An iteration process in which these general considerations have been taken into account may be chosen to consist of an outer Newton iteration on the circulation Γ, and two inner iteration procedures, one for the calculation of corrections outside

SHOCK CELLS
BEFORE MGR - SWEEP

SHOCK CELLS
AFTER CONVERGENCE

CELLS THAT SHOULDS
CHANGE FROM SUBSONIC
TO SUPERSONIC

CONVERGED SHOCK AT
END OF MGR - SWEEP

SHOCK AT START
OF MGR - SWEEP

STREAMLINE   S

GRID CELLS
AND POINTS

AEROFOIL IMAGE

φ, Φ

φ USUALLY COMPUTED
AFTER MGR - SWEEP

SHOCK   SHOCK

VELOCITY OVERSHOOT
(OR UNDERSHOOT)

CONVERGED φ
AFTER
MGR - SWEEP

$d\varphi$

$\varphi = \Phi + d\varphi$

φ AT START OF
MGR - SWEEP

$d\varphi$ φ

S

LINEAR CORRECTION EQUATIONS OR
TRUNCATION - ERROR ESTIMATES
FROM Φ (SHOCK POSITION FIXED)

$d\varphi$ USUALLY
COMPUTED
AFTER
MGR - SWEEP

$d\varphi$

DESIRED $d\varphi$

$d\varphi$

S

LINEAR CORRECTION EQUATIONS (FOR
LINEAR MGR - PROCESSES) OR
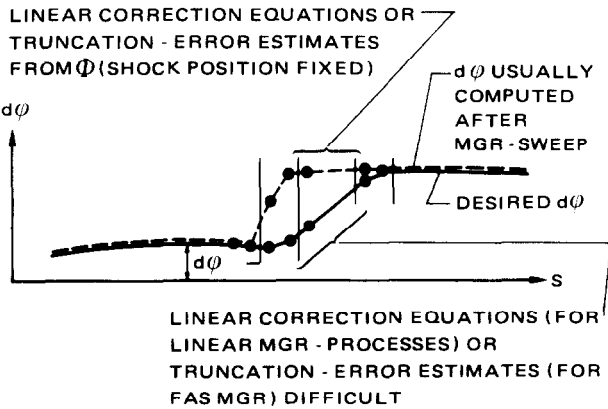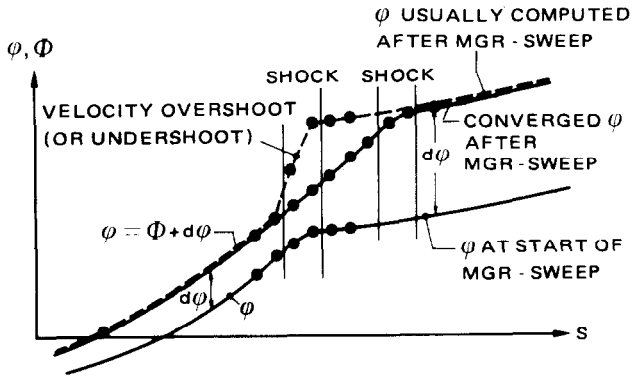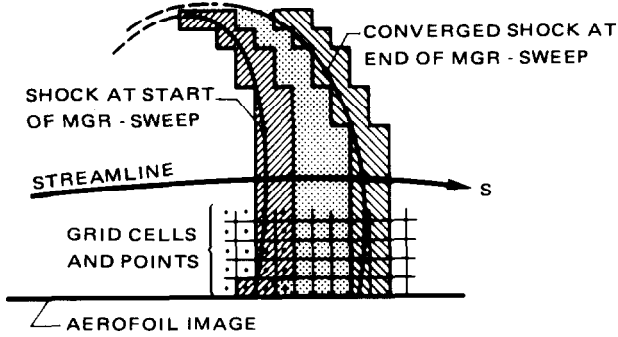TRUNCATION - ERROR ESTIMATES (FOR
FAS MGR) DIFFICULT

FIGURE 6

shocks (whereby multigrid relaxation is applied), and one for the update of shock positions. This combination of iteration procedures may be represented by the following algorithm:

initialise φ, Γ_a;
until Γ_a accurate enough **do**
begin until flow equations at fixed Γ_a are solved **do**
   begin improve φ at fixed Γ_a by one multigrid cycle;
      improve shock positions with partial relaxation sweeps;
   end of iteration at fixed Γ_a
      compute error in Kutta condition;
      improve circulation estimate Γ_a;
end of outer Newton iteration on Γ.

The outer Newton iteration on the circulation is based on a split of the finite-difference equation system of the form

$$L\{\varphi(\Gamma)\} = Q, \tag{31}$$

$$\{\partial\varphi(\Gamma)/\partial\xi\}_{te} = 0, \tag{32}$$

where the last equation is the Kutta condition, and the first one represents all other equations. The solutions $\varphi(\Gamma_a)$ of the nonlinear system (31) alone define a (nonlinear) relation between Γ_a and $\{\partial\varphi(\Gamma_a)/\partial\xi\}_{te}$; see Fig. 7 for an illustration. Kutta condition (32) means that we are interested in the value Γ on the horizontal axis. We may iterate to this value as shown in the figure. The slopes needed in this Newton iteration process are estimated by numerical differentiation. On a fixed grid, three to four steps are usually sufficient to fix the lift coefficient to about three significant figures.

In each step of the outer Newton iteration process to Γ, nonlinear equation system (31) has to be solved for a fixed estimate Γ_a of the desired value of the circulation. This is done iteratively. In each iteration step, the solution is first improved outside
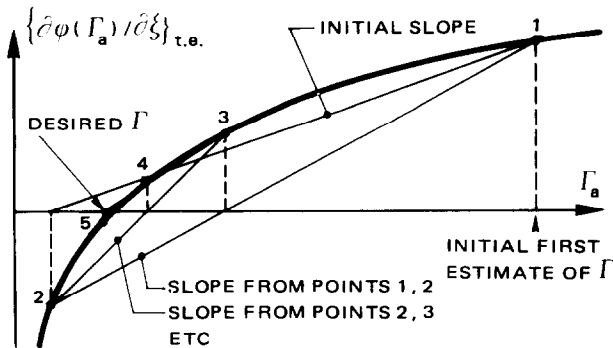

FIGURE 7

shock layers by one multigrid relaxation cycle (see Section 4), whereby shock positions hardly vary. This multigrid relaxation cycle is followed by an update of shock positions with nonlinear relaxation sweeps on the finest grid in (small) subdomains around shocks (partial relaxation sweeps). In the first partial relaxation sweep, the subdomains to be relaxed cover only shock cells. In each subsequent sweep, the subdomains are enlarged by one row of cells upstream, above, below, and downstream of the subdomain relaxed in the previous sweep. This enlargement is necessary because partial relaxation on fixed subdomains may lead to divergence due to an increase of residuals at the boundaries of the subdomain.

The termination of the iteration to a solution of (31): $L\{\varphi(\Gamma_a)\} = Q$ for a fixed estimate of Γ_a of the desired circulation is based on a test combining two criteria. When the circulation is not yet accurate enough, the iteration terminates as soon as the value of $\{\varphi_\xi\}_{te}$ is so accurate that it may be reliably used to improve the circulation to a better estimate. When the circulation is accurate enough, however, the iteration to a solution is terminated when a norm of the residuals of the mass conservation equations of the cells has become small enough. This test strategy drives the circulation as fast as possible to its final value.

A suitable norm of the residuals was found to be the maximum norm (see (1))

$$R_{\max} = \max_{i,j} \{(\eta_j/\eta_u)^2 \, |\nabla_{i,j}^{\mathrm{T}} F^d|\} \, h^m. \tag{33}$$

The scaling of the residuals $\nabla_{i,j}^{\mathrm{T}} F^d$ by η_j^2 reflects the fact that the residuals of sufficiently accurate approximate solutions are of order $\eta^{-2} O(h^m)^2$; hence, they are allowed to grow with $\eta \downarrow 0$. The scaling by the mesh size h^m makes the norm nondimensional (hence, mesh-size independent). A maximum norm is preferred over a rms-norm, because an rms-norm does not show that in certain stages of the iteration process large residuals may occur in very small regions. For example, when iterating at fixed Γ_a, after each multigrid relaxation sweep the residuals of shock cells are usually at least an order of magnitude larger than elsewhere in the flow due to velocity overshoots (or undershoots) as sketched in Fig. 6. Since rms-norms (or average absolute-value norms) do not efficiently measure large residuals in such small regions, they cannot be used safely in termination tests of loops.

In subsonic flow calculations, the partial relaxation sweeps are suppressed.

The Newton iteration process on a grid is started with an initial approximation of the potential that is computed by solving the nonlinear finite-difference equation system (31, 32) on a coarser grid (mesh size doubled). This is repeated on a sequence of three to four grids. On the coarsest grid of this sequence, the entire calculation is started with a uniform-flow potential having no circulation.

4. MULTIGRID RELAXATION CYCLES

The multigrid relaxation cycles used in this study have a general structure closely resembling the cycle C algorithm of Brandt [21]. Its general structure is presented in

Fig. 8a. It may be seen that the cycle starts with a linearization of the flow equations on the finest grid so that the whole cycle effectively represents one (approximate) Newton iteration step.

A few details of the implementation of this multigrid relaxation cycle are of special interest:

(i)   The restriction operations are applied to the complete linearized conservation equations instead of residuals. This is done in such a way that the equation

LEVEL	MESH
1	h^1
2	$\dfrac{h^1}{2}$
3	$\dfrac{h^1}{4}$
$m-2$	$4\,h^m$
$m-1$	$2\,h^m$
m	h^m

(L)   LINEARIZATION OF FLOW EQUATIONS

↑   RESTRICTION OF LINEARIZED FLOW EQUATIONS

⇒   INITIALIZATION OF CORRECTION POTENTIAL $d\varphi^1$ TO ZERO

(R)   RELAXATION OF LINEARIZED EQUATIONS, R SWEEPS

↓   BILINEAR PROLONGATION OF CORRECTION POTENTIAL

➡   ADDITION OF CORRECTION POTENTIAL TO FULL POTENTIAL
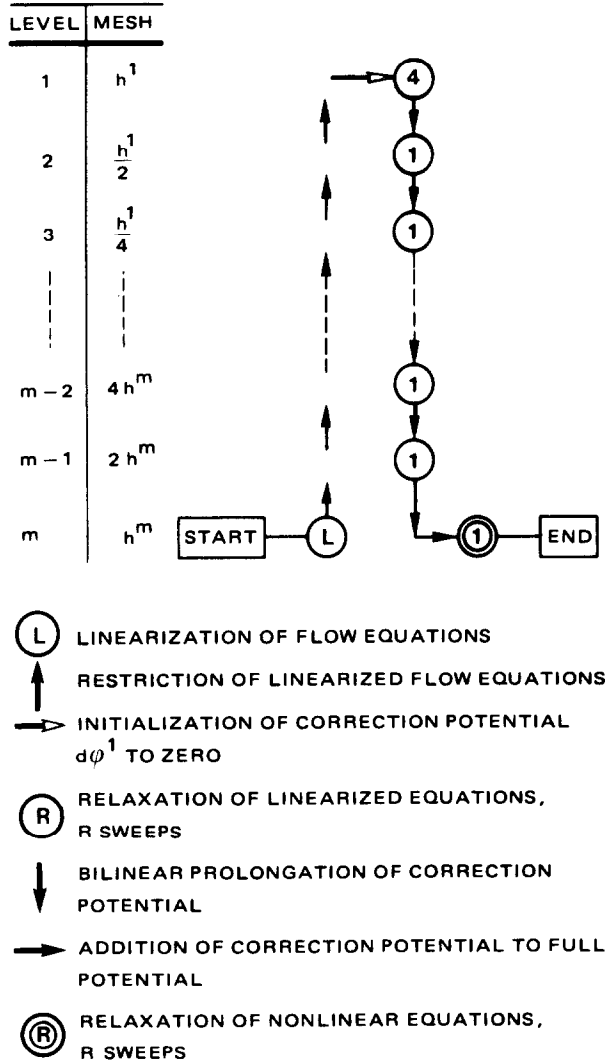
(Ⓡ)   RELAXATION OF NONLINEAR EQUATIONS, R SWEEPS

FIGURE 8a

system on the coarser grids may be interpreted as approximations to the mass conservation equations on the finest grid.

(ii)   Certain stability properties of the linearized flow equations are transferred in a controlled way to the coarser grid equations. See Section 5 for more details.

As shown in Fig. 8a, each multigrid relaxation cycle starts with a linearization of the nonlinear flow-equation system (31) on the finest grid around a given approximate solution ϕ^m. The result is a linear first-variation equation system for a first-variation potential $d\varphi^m$ on the finest grid,

$$\varphi^m = \phi^m + d\varphi^m, \tag{34}$$

$$C^m \, d\varphi^m = dR^m \equiv Q^m - L^m\{\phi^m\}. \tag{35}$$

The long-wavelength part of the correction $d\varphi^m$ will be computed on the coarser grids of the grid sequence. This requires the definition of equation systems

$$C^n \, d\varphi^n = dR^n, \qquad n = m - 1,\ldots, 1, \tag{36}$$

for these long-wavelength parts on the coarser grids by a restriction process. In order to obtain simple restriction rules based on the interpretation of linearized equation system (35) as a system of mass conservation equations and boundary conditions, the grids are chosen staggered so that four cells of a grid coincide with one cell of the nextcoarser grid; see Fig. 8b. Then the equation systems $C^n \, d\varphi^n = dR^n$ may be defined recursively from the one on the finest grid.

At each cell of a grid H^n, the first-variation equation is assumed to be known and to have the form:

$$\nabla^{nT}_{i,j} \, dF^{dn} = dR^n_{i,j}, \tag{37}$$

$$dF^{dn} = dF^n - dF^{an} + dF^{arn}, \tag{38}$$

$$dF^n = P^n \, \nabla^n \, d\varphi^n, \tag{39}$$
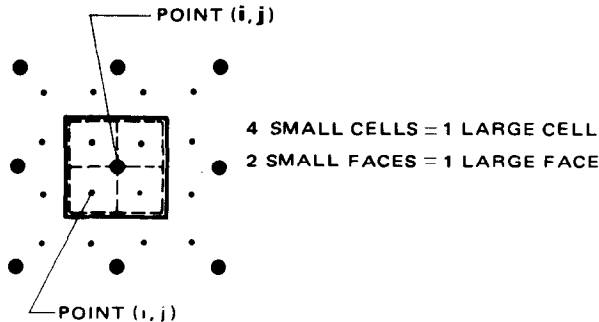
$$dF^{an} = A^n \, \nabla^n \, d\varphi^n, \tag{40}$$

4 SMALL CELLS = 1 LARGE CELL
2 SMALL FACES = 1 LARGE FACE

FIGURE 8b

where, on the finest grid $(n = m)$, the $dR_{i,j}^n$ are residuals of ϕ in (1):

$$dR_{i,j}^m = -\nabla_{i,j}^{m\text{T}} F^{dm}. \tag{41}$$

Here dF, dF^a, and dF^{ar} are the first variations of F, F^a, and F^{ar} around ϕ so that, on the finest grid, P^m and A^m may be shown to be the 2×2 matrices

$$P^m = [\rho h\{G - M^2 UU^\text{T}/q^2\}]^m, \tag{42}$$

$$A^m = 0, \qquad \text{if} \quad M \leqslant 1,$$

$$= [\rho h(1 - M^2)(UU^\text{T}/q^2)]^m, \qquad \text{otherwise.} \tag{43}$$

Each equation

$$\nabla_{i,j}^{(n-1)\text{T}} dF^{d(n-1)} = -dR_{i,j}^{(n-1)} \tag{44}$$

of a large cell $(\mathbf{i,j})$ on a grid H^{n-1} (see Fig. 8b) is defined from the four corresponding equations (37) on grid H^n by requiring that the coarse-grid equation should represent a mass conservation equation for the long-wavelength content $d\varphi^{n-1}$ of a suitable class of correction grid functions $d\varphi^n$. From this requirement, restriction rules for the residues and the coefficient matrices are readily derived with mass-flux considerations. For example, the mass flux through the face $(\mathbf{i, j} + \frac{1}{2})$ of the large cell $(\mathbf{i,j})$ in Fig. 8b should be equal to the total mass flux of the two corresponding faces of the small cells, giving

$$(P \nabla d\varphi)_{\mathbf{i,j}+1/2}^{n-1} = \tfrac{1}{2}[(P \nabla d\varphi)_{i,j+3/2}^n + (P \nabla d\varphi)_{i+1,j+3/2}^n]. \tag{45}$$

This should be true for the long-wavelength content in $d\varphi^n$. For the long-wavelength content, the three gradients in (45) are about equal:

$$(\nabla d\varphi)_{\mathbf{i,j}+1/2}^{n-1} \cong (\nabla d\varphi)_{i,j+3/2}^n \cong (\nabla d\varphi)_{i+1,j+3/2}^n, \tag{46}$$

so that an equation for the coefficient matrix P on the coarse grid is found:

$$P_{\mathbf{i,j}+1/2}^{n-1} = \tfrac{1}{2}(P_{i,j+3/2}^n + P_{i+1,j+3/2}^n). \tag{47}$$

Similar arguments are used to define the other coefficient matrices at the cell-face centres on the grid H^{n-1}. The residues are readily restricted by applying a discrete version of Gauss' theorem.

From (47) and similar formulas it follows that the coefficients at the cell-face centres are determined with coefficient-weighting. Residual weighting is also applied: each residual $dR_{\mathbf{i,j}}^{n-1}$ on the coarse grid turns out to be a weighted average of the residuals of the four smaller cells on the next finer grid that are covered by the coarse-grid cell $(\mathbf{i,j})$.

The linearized forms of Neumann boundary conditions (27), (28) are restricted to coarser grids in a similar way as illustrated by (45)–(47).

When the equation system $C^m d\varphi^m = dR^m$ for the desired correction $d\varphi^m$ of the

potential has been restricted to the coarser grids, $d\varphi^m$ is estimated. This is done by a recursive process involving (on each grid) improvement of $d\varphi^n$ by line relaxation and subsequent prolongation to the next finer grid by bilinear interpolation. The process starts on the coarsest grid by putting the initial correction potential $d\varphi^1$ equal to zero. When a $d\varphi^{m-1}$ has been prolonged to a $d\varphi^m$ on the finest grid of the grid sequence, $d\varphi^m$ is first added to the last potential ϕ^m to a new ϕ^m; this new potential is subsequently improved by nonlinear line relaxation over the entire finest grid. This nonlinear relaxation on the entire finest grid terminates the multigrid cycle.

On each grid, one line-relaxation sweep over the grid is sufficient. On the coarsest grid H^1, it is desirable to make more sweeps, however, to obtain a reasonable estimate of $d\varphi^1$. Four sweeps were found a suitable number in applications.

5. STABILITY

From numerical experiments it was found that both the application of mass-flux-vector splitting as well as calculation of gradients, velocities, and densities at cell-face centres are necessary to obtain good stability properties. As far as stability at sonic lines and shocks is concerned, much insight may be obtained from (9)–(13).

It is also very helpful to analyze the structure of the coefficient matrices in the first-variation equation (37) of each individual nonlinear discrete mass conservation equation (1). A necessary condition for stability of the nonlinear finite-difference equation system is stability of each individual first-variation equation (37), because (37) is an exact linearization of (1). The last property is a consequence of the computation of q and ρ from $\nabla\varphi$ at cell-face centres (instead of at cell corners, as usually is done). The stability of each first-variation equation (37) depends on the eigenvalues of the matrices $P^m - A^m$ and A^m; see (42), (43). It may be shown that in subsonic flow P^m is positive definite and A^m is zero while in supersonic flow, $P^m - A^m$ and A^m are both precisely semi-definite, with A^m having one negative eigenvalue corresponding to the streamline direction U/q, and $P^m - A^m$ having one zero eigenvalue also corresponding to the streamline direction U/q. This may be concluded from the following factorization for supersonic flow of the mass-flux vectors and matrices (the superscript m for the grid is omitted):

$$F - F^a = hH^{-1}V \begin{bmatrix} \rho^* q^*/q & 0 \\ 0 & \rho \end{bmatrix} V^{\mathrm{T}} H^{-1\mathrm{T}} \nabla\varphi, \tag{48}$$

$$F^a = hH^{-1}V \begin{bmatrix} (\rho q - \varphi^* q^*)/q & 0 \\ 0 & \rho \end{bmatrix} V^{\mathrm{T}} H^{-1\mathrm{T}} \nabla\varphi, \tag{49}$$

$$P - A = hH^{-1}V \begin{bmatrix} 0 & 0 \\ 0 & \rho \end{bmatrix} V^{\mathrm{T}} H^{-1\mathrm{T}}, \tag{50}$$

$$A = hH^{-1}V \begin{bmatrix} \rho(1 - M^2) & 0 \\ 0 & 0 \end{bmatrix} V^{\mathrm{T}} H^{-1\mathrm{T}}, \tag{51}$$

where V is the orthonormal matrix of Eq. (8), and H is the Jacobian of the mapping from the computational to the physical plane, so that $G = H^{-1}H^{-1\mathrm{T}}$. Mass-flux-vector splitting leads thus to an exact separation of the positive and negative eigenvalues of the matrix P associated with the first-variation $dF = P \nabla \, d\varphi$ of the mass-flux vector $F = \rho h U$. The positive eigenvalue in the part $P - A$ suggests central differencing $dF - dF^a$; the negative eigenvalue in the part A suggests upstream differencing for F^{ar} and dF^{ar}.

The factorizations follow directly from the relation

$$[\varphi_s \; 0]^{\mathrm{T}} = \mathrm{V}^{\mathrm{T}} H^{-1\mathrm{T}} \nabla \varphi$$

(this follows from the chain rule for differentiation and from $\varphi_n = 0$), so that, together with (4), (8), we obtain

$$U/q = H^{-1} V [1 \; 0], \tag{52}$$

$$UU^{\mathrm{T}}/q^2 = H^{-1} V \begin{bmatrix} 1 & 0 \\ 0 & 0 \end{bmatrix} V^{\mathrm{T}} H^{-1\mathrm{T}}. \tag{53}$$

It will be seen from the results to be presented that approximately normal shocks are very steep. Detailed analysis of shock operators shows that this is a direct consequence of the eigenvalue of $P - A$ corresponding to the streamline direction being zero, while $F - F^a$ has a constant sonic streamline component; see (11), (48), and (52). The last property means that the central-difference part of mass-conservation equation (1) for cells just ahead of approximately normal shocks are independent of the large φ_{ss} in the shock. On fine grids, the Jameson artificial viscosity also has this property if the coefficients in this viscosity are evaluated at cell centres.

Mass-flux-vector splitting as presented here has been extensively tested numerically and was found useful for approximately normal shocks because the matrix UU^{T}/q^2 in the mass-flux vector F^a is the image in the computational plane of a unit vector along the streamline in the physical plane; see (52). It may be expected that steep oblique shocks will at least require replacement of UU^{T}/q^2 by some matrix $\tilde{U}\tilde{U}^{\mathrm{T}}$, where $\tilde{U}$ is the image in the computational plane of a unit vector approximately normal to the oblique shock.

The definiteness properties of the matrices $P^m - A^m$ and A^m are used for the design of diagonally-dominant tridiagonal matrices to be applied in line relaxations; see Section 6 below. The definiteness properties are transferred to coarser grids by the simple restriction rules of form (47), so that on coarser grids these properties are easily traced. This is important for the convergence of relaxations on the coarser grids.

6. LINE RELAXATION

In each multigrid relaxation sweep and on each grid H^n of the grid sequence, an approximation of the solution of first-variation equation system (36): $C^n \, d\varphi^n = dR^n$

or of nonlinear equation system (31): $L^n(\varphi^n(\Gamma_a)) = Q^n$ is improved by one or a few line relaxation sweeps over the entire grid. Relaxation in the downstream direction is applied; a sweep over the lower part of the aerofoil is followed by a sweep over the upper part.

Tridiagonal equation systems to be used in line relaxation sweeps may be derived in various ways. For example, Jameson used an analysis of a pseudo-time-dependent process to derive these relaxation equations [23]. The relaxation equations may also be derived directly from the first-variation equations, however, by considering relaxation on each individual grid line as a crude Newton iteration step at that grid line.

The derivation of the relaxation equation system of each i line starts thus with the assumption that, for the potential values on the i line, a correction problem has to be solved. We may put on the entire grid

$$dC^n = d\varphi^n - d\phi^n \qquad \text{or} \qquad dC^n = \varphi^n - \phi^n, \tag{54}$$

where $d\phi^n$ or ϕ^n are given estimates of potentials and dC^n is the correction to be computed from a relaxation equation system. Initially, this system has the same form as the first-variation equation (37)–(40), with the mass-flux vectors dF^n, dF^{an}, and dF^{arn} now depending on dC^n instead of on $d\varphi^n$:

$$dF^n = P^n \nabla^n dC^n, \tag{55}$$

$$dF^{an} = A^n \nabla^n dC^n, \tag{56}$$

while the right-hand side is replaced by the residual of $d\phi^n$ or ϕ^n in (37) or in (1). This equation system is subsequently crudely approximated to a simple relaxation system for the calculation of values of $dC_{i,j}$ on line i, with a tridiagonal diagonally-dominant coefficient matrix. The approximation process consists of the following steps:

(i)   Finite-difference formulas with asymptotic scaling are replaced by the usual difference formulas.

(ii)   Second-order cross differences $dC^n_{\xi n}$ are removed by zeroing the off-diagonal elements in the matrices $P^n - A^n$ and A^n. The only differences that remain are those of $dC^n_{\xi\xi}$ and dC^n_{nn} multiplied by diagonal elements of $P^n - A^n$ and A^n with a known sign (see the discussion in Section 5 about the definiteness properties of $P^n - A^n$ and A^n).

(iii)   Retarded fluxes dF^{arn} representing inflow into a cell are zeroed. This simulates, for each cell in the supersonic zone, a zero initial condition if the calculation of values of $dC^n_{i,j}$ on line i is considered to be an isolated subproblem.

(iv)   Corrections $dC^n_{i+a,j+\beta}$ at points $(i + a, j + \beta)$ not yet updated in the current sweep are zeroed. This simulates a Dirichlet boundary condition in the subproblem.

The resulting tridiagonal system is augmented by a formula for the improvement of the Neumann boundary condition, derived by linearizing nonlinear condition (28),

and (crudely) approximated by one-sided differences at the point (i, J) in such a way that diagonal dominance is preserved.

The tridiagonal equation system derived in this way from the linear first-variation equations turns out to be practically identical to that of Jameson [3, 5, 23] if the flow is subsonic or supersonic, however, without Jameson's subsonic or supersonic relaxation factors. At sonic lines and shocks, a comparison with Jameson's formulas was not possible because of a lack of published results. The relaxation equation of sonic or shock cells turns out to be different from those elsewhere in the flow if they are derived from the first-variation equation.

Relaxation factors were not used in the calculation results presented below, except at sonic cells where underrelaxation was applied.

7. RESULTS OF NUMERICAL EXPERIMENTS

From a large number of numerical experiments, a number of cases have been selected. This selection permits a separate analysis of the effect of circulation changes, grid changes, shock-position variations, etc.

All results presented were produced by calculations made on three successive grids of size 34×10, 66×18, 130×34, which are numbered 2, 3, and 4. Each 130×34 grid is similar to that of Fig. 3. Multigrid sweeps for the calculations on grid 2 used two grid levels, multigrid sweeps for grid 3 used three, and multigrid sweeps for grid 4 used four grid levels.

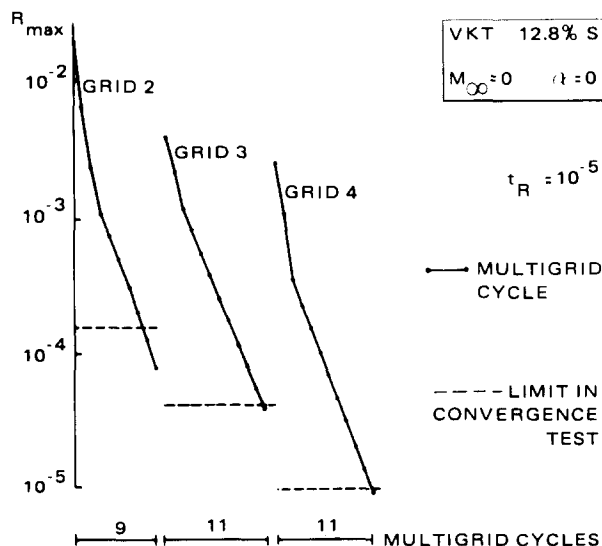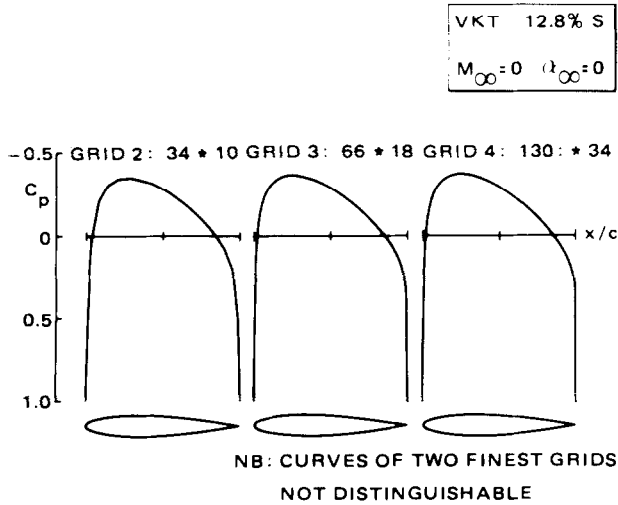Figures 9a and b concern the flow around a symmetrical 12.8% thick

FIGURE 9a

FIGURE 9b

Karman–Trefftz aerofoil at $M_\infty = 0$, $\alpha_\infty = 0$ (linear problem, no circulation). Two conclusions follow from the convergence history.

(i)   The multigrid convergence rate is good (about 0.6 per multigrid cycle).

(ii)   The residual norm increases when a solution is prolonged to a next-finer grid to serve as the starting solution. This is due to a poor resolution of the coarser grids at the leading edge, as will be evident from Fig. 3 when 4 or 16 cells of the finest grid are grouped together to one cell of a coarser grid.

Results of the incompressible flow around the same Karman–Trefftz aerofoil, at an incidence α_∞ of $10°$, are presented in Fig. 10a and b. It is seen that:

(i)   changes in circulation, in particular large changes, may lead to large increases of residual norms. This is due to large changes of the solution at the leading edge.

(ii)   the grids 2 and 3 are too coarse at the leading edge to permit a reasonably accurate calculation of the expansion of the flow at the leading edge.

(iii)   the multigrid convergence rate is good (about 0.6 per multigrid cycle).

Results for a high-subsonic flow are presented in Fig. 11a and b (NACA0012, $M_\infty = 0.63$, $\alpha_\infty = 2°$). The addition of subsonic nonlinearity does not lead to new conclusions.

The added complication of a shock in the calculation process is first considered for a nonlifting case with a moderate shock (NACA0012, $M_\infty = 0.8$, $\alpha_\infty = 0$). Results are presented in Fig. 12a and b. New conclusions are the following:

(i)   After each multigrid relaxation cycle, and on all but the coarsest grid 2, the maximum norm of the residuals, Eq. (33), is usually found to be increased by an
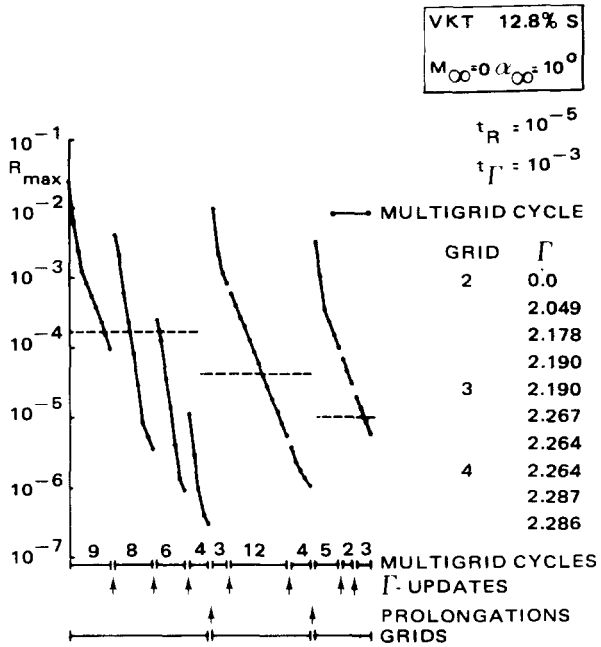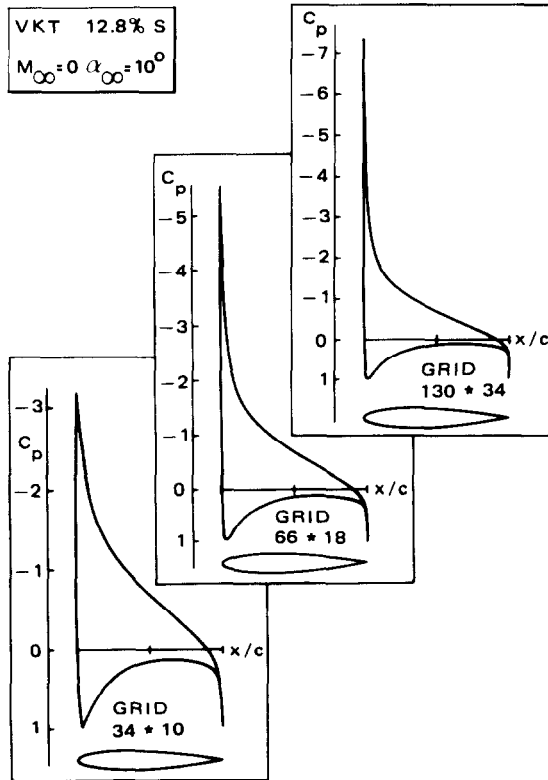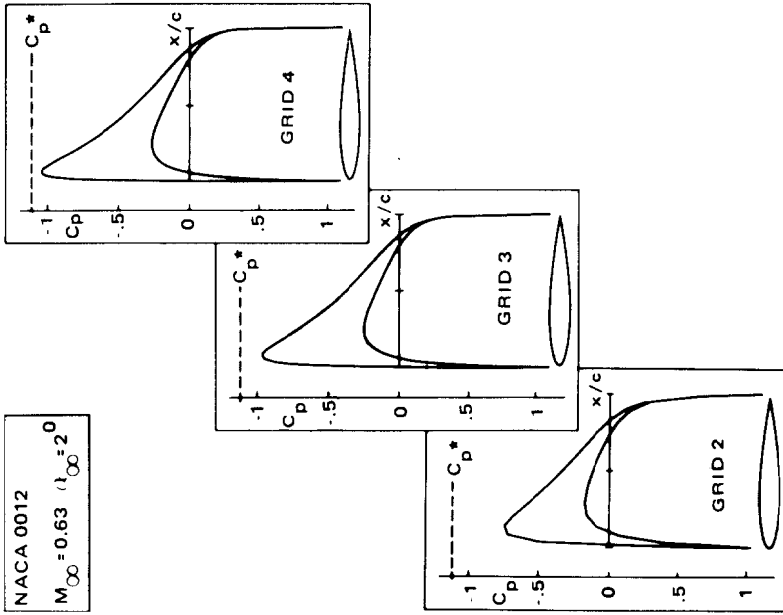
$t_R = 10^{-5}$

$t_\Gamma = 10^{-3}$

— MULTIGRID CYCLE

GRID	Γ
2	0.0
	2.049
	2.178
	2.190
3	2.190
	2.267
	2.264
4	2.264
	2.287
	2.286

10^{-1}

R_{max}

10^{-2}

10^{-3}

10^{-4}

10^{-5}

10^{-6}

10^{-7}

9 8   6   4 3 12   4 5 2 3   MULTIGRID CYCLES

↑   ↑   ↑   ↑   ↑   ↑↑ ↑ Γ-UPDATES

↑   ↑   PROLONGATIONS

GRIDS

FIGURE 10a

C_p

−7

−6

−5

−4

−3

−2

−1

0

1

x/c

GRID
130 * 34

C_p

−5

−4

−3

−2

−1

0

1

x/c

GRID
66 * 18

−3

C_p

−2

−1

0

1

x/c

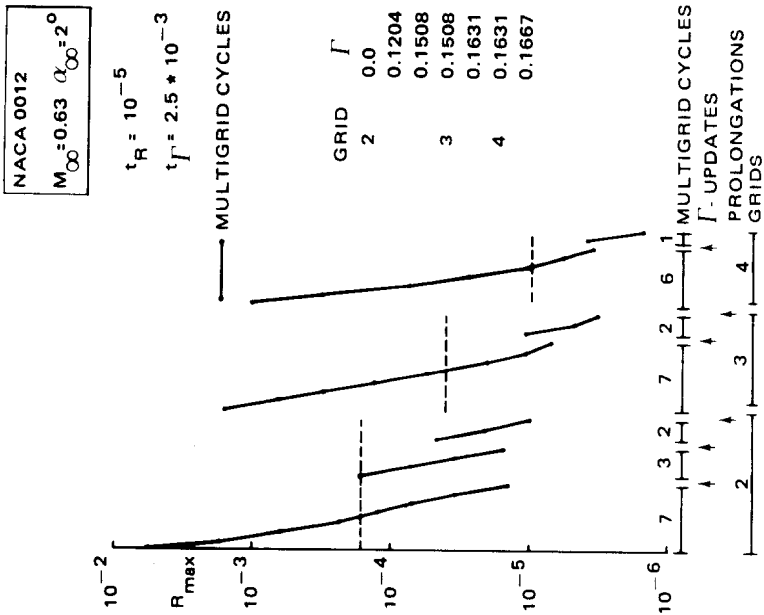GRID
34 * 10

FIGURE 10b

FIGURE 11b

FIGURE 11a

order of magnitude. This annoying behaviour of the maximum norm is due to velocity overshoots or undershoots at shocks, as discussed in Section 3 and illustrated in Fig. 6. A typical example of a velocity overshoot is presented in Fig. 12c. (This figure is the result of a somewhat different algorithm not presented in this report; the velocity overshoot effect is representative, however.) As discussed, the velocity overshoot is due to a tendency of multigrid relaxation cycles to keep the shock position fixed. See also Jameson's remark [11, p. 125] about "the appearance ahead of the shock of a temporary overshoot," and the corresponding flat segment in the convergence history in his Fig. 2b. This implies that there must be large residuals in small zones keeping his average-absolute-value norm temporarily about constant.

(ii)   The velocity overshoots can be reliably transformed with partial relaxation sweeps on the current finest grid to appropriate shock displacements; partial relaxation usually reduces the residual norm considerably.

(iii)   The lack of resolution at the leading edge on the coarser grids leads to too small flow expansion over the leading edge and to too forward shock positions. It may be expected that improvement of the resolution at the leading edge on grids 2 and 3 will lead to better pressure distributions so that a smaller calculation effort to improve shock positions is required (see [24]).

A transonic case with lift is presented in Figs. 13a and b (NACA0012, $M_\infty = 0.75$, $\alpha_\infty = 2°$). This case has also been computed in [7, 11]. There are no important new points to be observed. The peak Mach number ahead of the shock is 1.37. Hence, for practical purposes, the shock is fairly strong. The shock obviously covers two cells; this is always true.
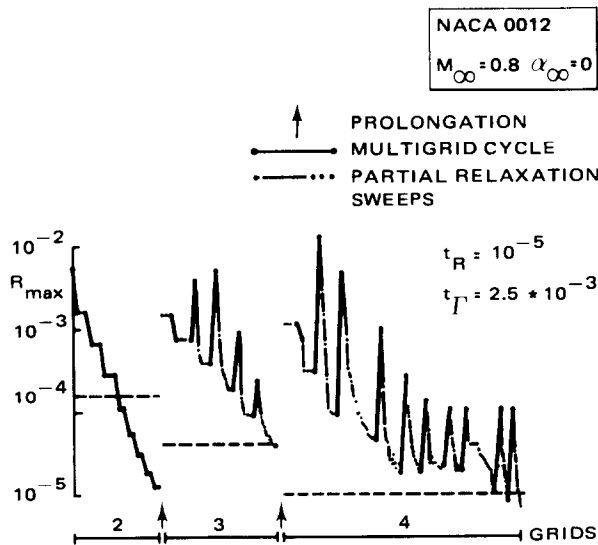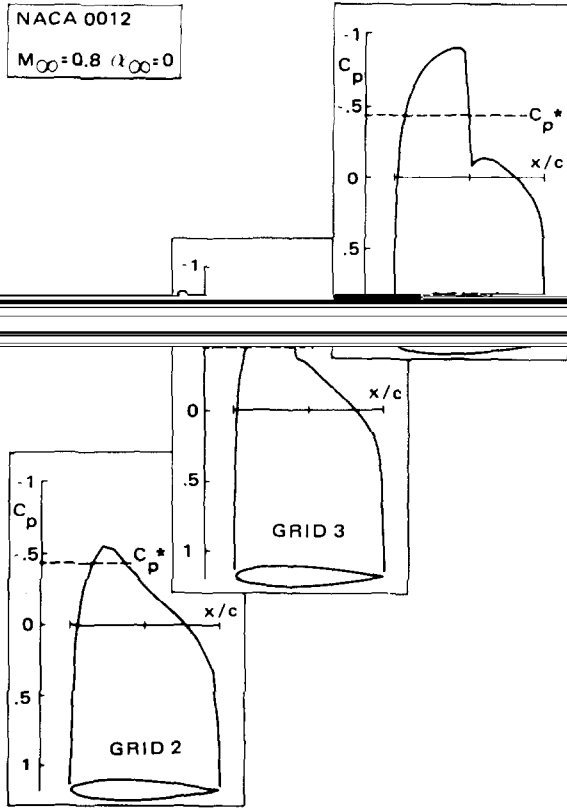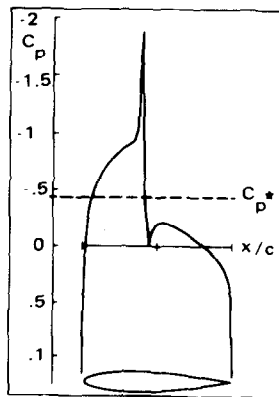

FIGURE 12a

NACA 0012

$M_\infty = 0.8$ $\alpha_\infty = 0$

FIGURE 12b

FIGURE 12c

TABLE I

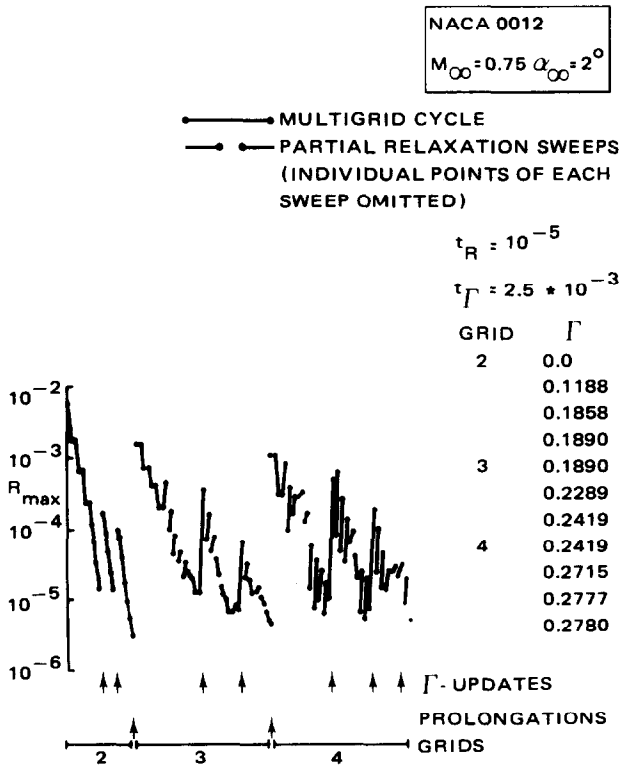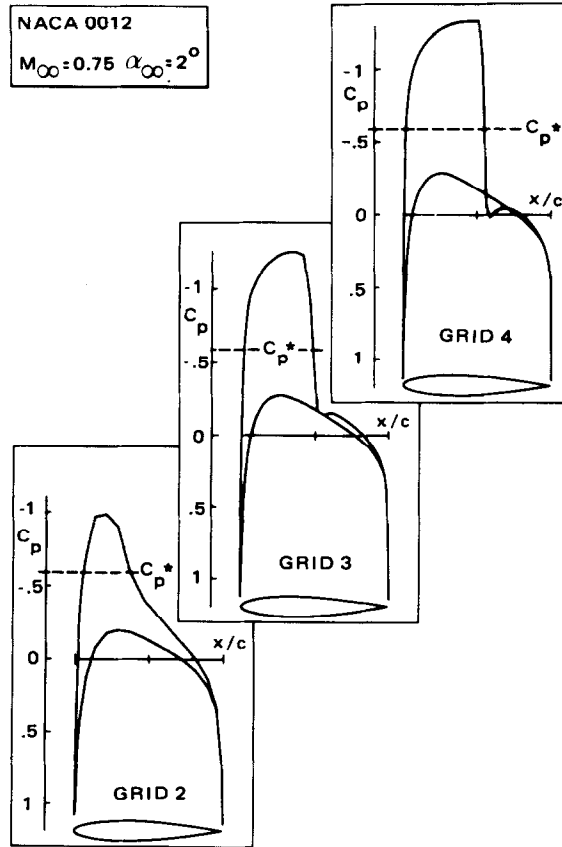| $(M_\infty, \alpha_\infty)$	Grid	Number of MGR cycles	Number of partial relaxation sweeps	CP-S per grid	Total CP-S
(0.63, 2°)	2	14	0	31	
	3	10	0	74	
	4	8	0	219	324
(0.8, 0)	2	8	14	23	
	3	5	30	64	
	4	10	122	680	767
(0.75, 2°)	2	21	29	58	
	3	23	68	231	
	4	25	278	1544	1833

FIGURE 13a

FIGURE 13b

Central processor times of the research code used for the numerical experiments are presented in Table I. These times were measured on the NLR Cyber 73-28 computer. The table illustrates that the algorithm is efficient for subsonic flows. For transonic flows, the computation times are too long. This is primarily due to the partial relaxation sweeps used to update shock positions. A continued search for improved shock-position update algorithms will be required.

Results of computations with various forms of artificial viscosity terms instead of split mass-flux-vectors are omitted. We found all artificial viscosity terms tested to have poor stability properties at sonic lines and/or shocks (in particular on coarse grids), and also at the tops of supersonic zones when corrections were large. This was due to the fact that the viscosity terms did not deliberately exclude expansion shocks.

8. CONCLUSIONS

From the results presented in this study it is evident that the introduction of multigrid methods in transonic potential-flow calculations is not a simple matter. A number of conclusions are clear from the present study, however.

(i) Circulation changes usually give rise to an increase of residual norms (Section 7).

(ii) Fast-solver algorithms are considerably more sensitive to nonlinear instability at shocks and sonic lines. This requires difference formulas with excellent stability properties. Such formulas are obtained with mass-flux-vector splitting (Section 2 and 5).

(iii) It will be hard to improve shock-wave positions by multigrid relaxation processes because multigrid relaxation is a linear or weakly nonlinear (FAS) correction process, while shock-wave displacement processes are highly nonlinear (Section 3, Fig. 6, Sect. 7). Usually, velocity overshoots or undershoots at shocks have to be eliminated during the calculation process.

(iv) In order to obtain a useful residual norm to be used in termination tests of loops, finite-difference formulas with asymptotic scaling have been used (Section 2, Eq. (33)). Compared to the usual finite-difference formulas, however, these are more expensive. There is a possibility that asymptotic scaling may be avoided if termination tests not using residual norms can be found.

(v) The algorithm was found to be reasonably robust in numerical experiments (Section 7). This conclusion is supported by theoretical results concerning the stability of the equation system (Section 5; Section 1, Eqs. (12) and (13).

Concluding, it can be said that for subsonic-flow calculations the algorithm was found to be quite efficient. For transonic-flow calculations with shocks, the algorithm was found to be reliable. More efficient procedures for the update of shock-positions are required however; these should be at least as robust (convergence guaranteed) as the preliminary procedure (partial relaxation near shocks) investigated in this study.

REFERENCES

1. E. M. MURMAN AND J. D. COLE, *AIAA J.* **9** (1) (1971), 114.
2. E. M. MURMAN, *AIAA J.* **12** (5) (1974), 626.
3. A. JAMESON, *in* "Proc. AIAA 2nd Comp. Fl. Dyn. Conf.," pp. 148–174, June 1975.
4. A. JAMESON AND D. A. CAUGHEY, *in* "Proc. 3rd Comp. Fl. Dyn. Conf.," pp. 35–54, June 1977.
5. D. A. CAUGHEY AND A. JAMESON, *AIAA J.* **17** (2) (1979), 175.
6. J. TH. VAN DER KOLK AND J. W. SLOOFF, "A Comparison of Computational Results for Transonic Flow around the ONERA-M6 Wing," NLR report prepared for GARTEUR AD(AG01) 1981 to be published.
7. A. RIZZI, "Numerical Methods for the Computation of Inviscid Transonic Flow with Shock Waves," FFA report prepared for GAMM workshop, Sept. 1979.

8. L. J. Fuchs, "Finite-Difference Methods for Plane Steady Inviscid Transonic Flows," Rep. TRITA-GAD-2, Stockholm, May 1977.
9. L. J. Fuchs, in "Proc. 1st Conf. Bound. Interior Layers/Comp. Asympt. Methods," Dublin, 1980.
10. J. C. South, Jr. and A. Brandt, "Application of a Multi-Level Grid Method to Transonic Flow Calculations, ICASE Rep. 76-8, 1976.
11. A. Jameson, in "AIAA 4th Comp. Fl. Dyn. Conf.," pp. 122–146, July 1979.
12. D. A. McCarthy and T. A. Rheyner, "A Multi-Grid Code for Three-Dimensional Transonic Potential Flow about Axisymmetric Inlets at Angle of Attack," AIAA Paper 80-1365, 1980.
13. B. Arlinger, "Multigrid Technique Applied to Lifting Transonic Flow Using Full Potential Flow Equation," SAAB–Scania Rep. L-0-1 B439, December 1977.
14. T. L. Holst, *AIAA J.* **17** (10) (1979), 1038.
15. T. J. Baker, "A Fast Implicit Algorithm for the Nonconservative Potential Equation," open forum presentation, AIAA 4th Comp. Fl. Dyn. Conf., July 1979.
16. D. Catherall, "Optimum Approximate-Factorisation Schemes for 2D Steady Potential Flows," AIAA Paper 81–1018, July 1981.
17. J. W. Boerstoel and L. J. Simons, "On the Approximate Solution of the Transonic Small Perturbation Equation with a Galerkin/Least-Squares Method and Bicubic Hermite Functions, NLR Rep. TR 78134 C, 1978, Confidential.
18. W. J. Piers and J. W. Slooff, in "Proceedings AIAA Comp. Fl. Dyn. Conf.," pp. 147–156, July 1979.
19. W. Hackbush, *Numer. Math.* **32** (1979), 83.
20. A. Brandt and N. Dinar, "Multigrid Solutions to Elliptic Flow Problems," ICASE Rep. 79-15, July 1979.
21. A. Brandt, *Math. Comp.* **31** (138) (1977), 333.
22. B. Engquist and S. Osher, *Math. Comp.* **34** (149) (1980), 45.
23. A. Jameson, *Comm. Pure Appl. Math.* **27** (1974), 283.
24. T. L. Holst and D. Brown, "Transonic Airfoil Calculations Using Solution-Adaptive Grids," AIAA Paper 81-1010, 1981.
25. A. Eberle, "Eine Methode finiter Elemente zur Berechnung der transonischen Potential–Strömung um Profile," MBB Rep. UFE1352(Ö), September 1977.
26. M. M. Hafez, J. South, and E. Murman, *AIAA J.* **17** (8) (1979), 838.